Simulation of thermoelectric properties of bismuth telluride single crystalline films grown on Si and SiO_2 surfaces

H. Kaddouri,[1] S. Bénet,[1] S. Charar,[2] M. Makowaska-Janusik,[3] J. C. Tedenac,[4] and I. V. Kityk[3]
[1]*LP 2A, Universite de Perpignan, Avenue de Villeneuve, 66860 Perpignan Cedex, France*
[2]*GES, UMR No. 5660, Universite Montpellier II, Place E. Bataillon, 34095 Montpellier Cedex 5, France*
[3]*Institute of Physics WSP, aleja Armii Krajowej 13/15, 42-200 Czestochowa, Poland*
[4]*LPCM-Université de Montpellier II, Place E. Bataillon, 34095 Montpellier Cedex 5, France*
(Received 14 February 2000; revised manuscript received 7 July 2000)

Self-consistent band-energy-structure calculations of the band-energy structure of Bi_2Te_3 single-crystalline films grown on SiO_2 and Si surfaces, with a thickness of about 1 μm, have been carried out in order to simulate thermopower behaviors. The norm-conserving pseudopotential method within the local-density approach was used. The interface crystalline structure was optimized using a molecular-dynamics geometry optimization, taking into account the electron-phonon anharmonic interaction. The influence of the Si and SiO_2 substrates on the structural, electron, and thermopower parameters of Bi_2Te_3 single crystalline films is studied. From the obtained band-energy parameters' Fermi energy, thermopower coefficients were calculated for different types of substrates. A good agreement between theoretical simulations and experimentally obtained data was found. In order to evaluate the role of the bulk structure, similar measurements have been done for the Bi_2Te_3 single crystals with appropriate carrier concentrations as well for the Bi_2Te_3 crystals covered by Si and SiO_2 substrates. The obtained data show the key role of intercrystalline interfaces in the observed phenomena. The correlation between the measured electro-optic coefficients and simulated thermoelectric parameters indicates the essential role of carrier transfer at the border between the interacting crystalline surfaces.

I. INTRODUCTION

Recently one could observe an increasing interest in Bi_2Te_3 materials, due to the fact that they possess promising thermoelectric properties at low temperature.[1] Simultaneously such materials may be applied for optical recording of information,[2] laser diodes,[3] etc. A large number of proposals was devoted to the creation of different kinds of corresponding superlattices consisting of bismuth-telluride-type layers.[4–6]

The main problem that essentially restrains their wide application is the absence of a materials engineering modeling for such kinds of structures coming from the band-energy-structure calculation. The updated band-energy calculations[7,8] were oversimplified, and the aforementioned works were performed without taking into account the spin-orbit interactions. In Ref. 9 the electronic structure of Bi_2Te_3 was studied within a framework of the density-functional-theory approach, including relativistic and spin-orbit corrections. However, these authors calculated only perfect bulk-like crystals. They did not perform calculations for single crystals grown on the Si or SiO_2 substrates. Because the latter substrates are usually used for the creation of effective thermoelectric devices such as small thermoelectric coolers, power generators, and thermal sensors,[10] we will present self-consistent band-energy calculations of the aforementioned films grown on Si and SiO_2 crystalline substrates. To clarify the role of the bulk structure contribution, we perform similar calculations for bulk Bi_2Te_3 crystals doped with the appropriate number of carriers, as well for Bi_2Te_3 crystals that cover the Si and SiO_2 substrates.

The investigated films were grown using the hot-wall epitaxy (HWE) method.[11] It is well known that film thickness as well as deposition temperature plays a key role in the thermoelectric power and electrical resistivity of the considered films.[12] At the same time one can guess that both the film thickness as well as the type of substrate should play essential roles in the observed band-energy-structure, anisotropy, and derivative electronic properties.

In the present work we perform self-consistent band-energy-structure calculations of Bi_2Te_3 single-crystal films deposited on Si or SiO_2 single crystallites. The approach is (i) grounded on a molecular-dynamics geometry optimization of the interfaces between the deposited crystalline films and substrates; further, (ii) it takes into account the intrafilm electron-phonon anharmonicity that essentially disturbs the existing potential, as well as (iii) band-energy calculations using the norm-conserving pseudopotential method within a framework of the local-density approximation approach with the inclusion of spin-orbit interactions. (iv) Finally, we perform evaluations of the Fermi energy as well the nonlinear optical susceptibilities and the corresponding thermoelectric constants.

The structure of the paper is as follows. In Sec. II we present a method of film preparation as well as nonlinear optical susceptibility measurements. Section III is devoted to molecular-dynamics simulations of the film-crystalline interfaces. A band-energy calculation method taking into account the electron-phonon interaction is described in Sec. IV. The result of the band-energy-structure calculations together with the Fermi energy electro-optic coefficient evaluations are presented in Sec. V. Here we also show a comparison between the calculated and experimentally obtained data.

0163-1829/2000/62(24)/17108(7)/$15.00 ©2000 The American Physical Society

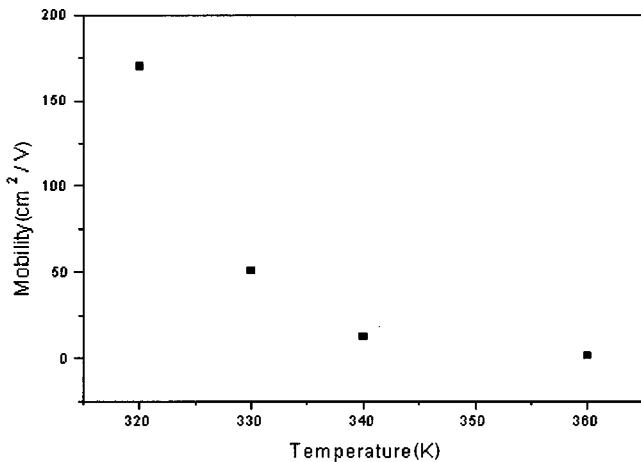

FIG. 1. Evolution of the carrier mobility vs the temperature of the substrates.

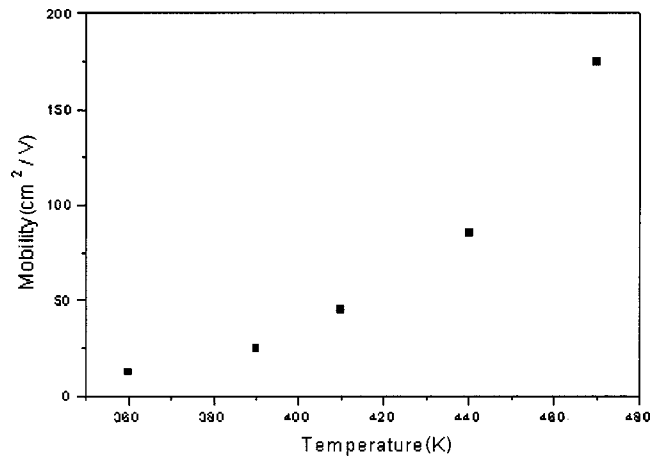

FIG. 2. Evolution of the carrier mobility vs the source temperature.

II. EXPERIMENT

A. Processing of the substrate

The chemical preparation of the substrate before the growth has a very large influence on the quality of thin films. The chemical processing of the substrates (SiO_2 and Si) that we used before each introduction into the HWE reactor consists of three stages: (1) cleaning in a solution of trichloroethylene then rinsing in methanol; (2) immersion in an acid concentrated in order to dissolve the oxide coating possibly formed (acid hydrofluoric for Si and the hydrochloric acid for SiO_2); and (3) rinsing in propanol-2 then drying with an inert gas. The substrates thus prepared are introduced into the HWE reactor, where they undergo a thermal processing at the growth temperatures for 1 h.

B. Case of the Bi_2Te_3 crystalline films deposited on SiO_2

In this case we noted a great correlation between the conditions of growth, the electric mobility, and the number of carrier. In Fig. 1 we can follow the evolution of mobility according to the temperature of the substrate when the temperature of the source is fixed at a value of 470 °C. In addition, we fixed the temperature of the substrate at 320 °C, and varied the temperature of the source of 360 °C by 470 °C (see Fig. 2).

C. Structural parameters of the films

In the case of a Si substrate, no simple correlation was established between the conditions of growth and the electrophysical properties of the layers. However, we noted that the greatest value of mobility is obtained for a substrate temperature of 340 °C, a source temperature equal to 470 °C$\mu_H = 22.7\ \mathrm{cm}^2/\mathrm{V\,s}$, a value of N of about $10^{20}\ \mathrm{Cm}^{-3}$, $a = 4.365$ Å, and $c = 30.238$ Å. In the case of films deposited on SiO_2, $a = 4.431$ Å and $c = 30.384$ Å.

D. Electro-optic setup

Electro-optic measurement were done for the wavelength of the CO_2 laser ($\lambda = 10.6\ \mu$m). The measurements were done separately for the Bi_2Te_3 crystallites, for the appropriate substrates (Si or SiO_2) as well for the crystallites grown on the crystallites. The Senarmont method developed for the layered crystal measurements was applied.[13] This method allows one to determine the birefringence with a precision up to the 6×10^{-5}. This enables one to determine the electro-optic coefficients with a precision of 0.2 pm/V. The measurements were made for the transverse geometry (the directions of electric field and the optical beam were perpendicular).

III. MOLECULAR-DYNAMICS GEOMETRY OPTIMIZATION

To perform a geometrical optimization, we applied the molecular-dynamics technique applied previously to different crystals, with the disturbed translational symmetry in the Refs. 14–16. We also used several approaches from the molecular-dynamics Becke method,[17] involving a semi-empirical contribution of the ''exact'' exchange. This method possesses relatively higher convergence with respect to the sizes of the basis sets, and allows one to vary continuously the intracluster as well as the intercluster distances playing a central role in corresponding structures.

The geometry optimization started from the interface between the Bi-Te film and the crystalline (Si or SiO_2) background. We began with a molecular-dynamics interface simulation of the fourth-neighboring layers (two from the crystallite sides and two from the film side). Thus we have taken into account about 40–60 atoms from both sides. The molecular-dynamics procedure was performed up to the achievement of the total minimum (per molecule) in a cluster chosen to be the same in all the composites. The latter was determined as a partial sum of the total energies for particular crystallites, for thin films, and for the aforementioned interface region.

In the second step we considered the next layers from the film side, and repeated the procedure for the total partial energy per molecule that corresponds to new volume of effective interface supercell (due to the restriction of the effective sub-cluster). The main condition that should be ensured at each step of the molecular basis renormalization is the condition of the *constant total energy per molecule*. That is similar to the well-known dynamics boundary derivative pro-

cedure of Refs. 14–16, with variable effective cluster sizes (dynamics boundary conditions) and the requirement of a minimum total-energy saving.

The step-by-step procedure was repeated as an iteration until the relative displacements of the successive layers were less than 0.04 nm. This corresponds to the atom position precision of the adopted model. We have performed an optimization for the film thickness of about 1 μm.

We revealed that the structure of the such crystalline film should be modulated with a modulation period about 8.6 nm for the Si(111) substrate 8.8 nm for the Si(100) substrates and 10.3 nm for the SiO_2 substrate (see Table II).

From Table II one can see that the silicon and silica substrate essentially modulate the Bi_2Te_3 single crystalline film structural parameters, and can additionally modulate the film structure with a period about 8.6–10 nm and relative atom shifts lying within 0.76% and 0.96%. Moreover, increasing the modulation period also stimulates decreased relative atomic shifts. The specimens grown on the SiO_2 should be of better quality compared with the Si-coated materials. The substrate orientations of silicon do not significantly influence the growth conditions.

It is worth noting that in the case of utilization of Si or SiO_2 crystallites deposited on the Bi_2Te_3 crystallites in the bulk, no modulation structure is observed. This fact essentially reflects the different total-energy minima of the bulk crystalline bismuth telluride and the silica and silicon crystallites. Thus conditions for growth of Bi_2Te_3 on the Si, or vice versa, play an important role.

One can predict that the observed mesoscopic crystallites of the films are a result of the revealed structural modulation. Physically this is a result of a competition between the intracrystalline long-range ordering and the interface disturbance. This is in agreement with the scanning electron microscopy measurements, that show that the ratio of the averaged crystallites on the silica to the silicon is approximately 1.43, which is supported by the data presented in Table II. The corresponding ratio for the two types of silicon-coated films is about 1.0. Similar effects in Ref. 18 were explained within a framework of the surface nucleation length. In our approach we use a molecular-dynamics geometry optimization that explains the same phenomena in a significantly stronger approach. For the case of the Bi_2Te_3 crystallites covered by Si or SiO_2, no such modulation was observed.

IV. BAND-ENERGY CALCULATIONS

A. Calculation method

At the beginning we carried out calculations for perfect crystals with the space group $D^5_{5d}(R3m)$, $Z=5$.[19] The notation of the symmetry points is presented in Fig. 3.

In order to obtain the band-energy structure, we first performed band-energy calculations using the self-consistent norm-conserving pseudopotential method.[20] Corresponding secular equations take the forms

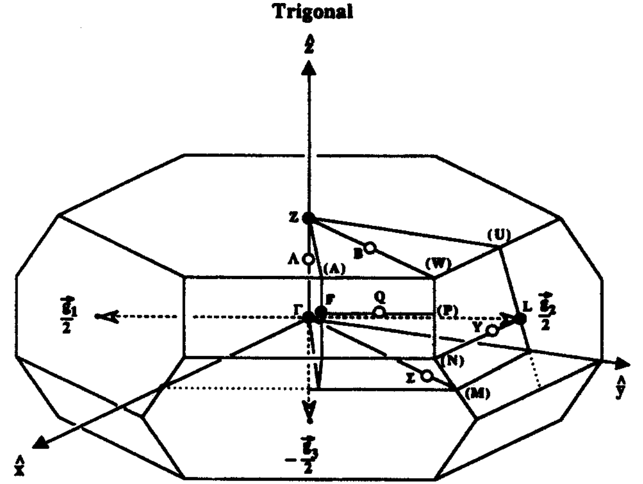

FIG. 3. Brillouin zone and indication of the symmetry points.

$$\|[h^2(\mathbf{k}+\mathbf{G}_n)^2/2m-E(\mathbf{k})]\delta_{n,n'} +\Sigma_\alpha V_\alpha(\mathbf{G}_b,\mathbf{G}_{n'})S_\alpha(\mathbf{G}_n,\mathbf{G}_{n'})\|=0,$$
$$\|[h^2(\mathbf{k}+\mathbf{G}_n)^2/2m-E(\mathbf{k})]\delta_{n,n'}+\Sigma_\alpha[V_\alpha(\mathbf{G}_n,\mathbf{G}_{n'}) +\Delta V_\alpha(\mathbf{G}_n,\mathbf{G}_{n'})]S_\alpha(\mathbf{G}_n,\mathbf{G}_{n'})\|=0, \quad (1)$$

where $S_\alpha(\mathbf{G}_n,\mathbf{G}_{n'})$ is a structural factor for the αth kind of atoms, $\mathbf{G}_n$, and $\mathbf{G}_{n'}$ are basic plane waves, and $V_\alpha(\mathbf{G}_n,\mathbf{G}_{n'})$ and $\Delta V_\alpha(\mathbf{G}_n,\mathbf{G}_{n'})$ are Fourier transforms of the perfect and interface disturbed crystals, respectively. All other symbols have their usual meanings. This Fourier transform can be written in the form.

$$V_\alpha(\mathbf{G}_n,\mathbf{G}_l)=\int d'\cdot\mathbf{r}\int d',\mathbf{r}'\exp(-iG_nr)[gq3V_\alpha(\mathbf{r},\mathbf{r}') +g_2V_{2\alpha}(\mathbf{r},\mathbf{r}')]\exp(-i\mathbf{G}_1\mathbf{r}'), \quad (2)$$

where g_1 and g_2 are weighting factors determining the perfect and interface disturbed structural components, respectively. The ionic form factors of the nonlocal pseudopotential part were calculated using the method described in Ref. 21.

An improvement of the band-energy-structure calculation was achieved by applying of the nonlocal exchange-correlation functional for valence electrons using the self-consistent norm-conserving pseudopotential method.[20] The accuracy of the eigenenergy calculations was better than 0.018 eV, and required the use of double precision options. An additional acceleration of the procedure was achieved by

TABLE I. Main electron parameters of the Bi_2Te_3 films.

	p-Bi_2Te_3/SiO_2	n-Bi_2Te_3/SiO_2	p-Bi_2Te_3/Si
T_{source} (°C)	470	470	470
$T_{substrate}$ (°C)	320	320	340
ρ (Ω cm)	2.08×10^{-3}	2.22×10^{-3}	1.30×10^{-3}
R_H	+0.353	−0.225	0.0296
μ_H (cm^2/V)	169	10.165	22.7
p,n (cm^{-3})	1.77×10^{19}	1.13×10^{19}	2.10×10^{20}
S (μV/K)	218	−204	150
Z (K^{-1})$_{at}$ 300 K	1.90×10^{-3}	1.56×10^{-3}	1.44×10^{-3}

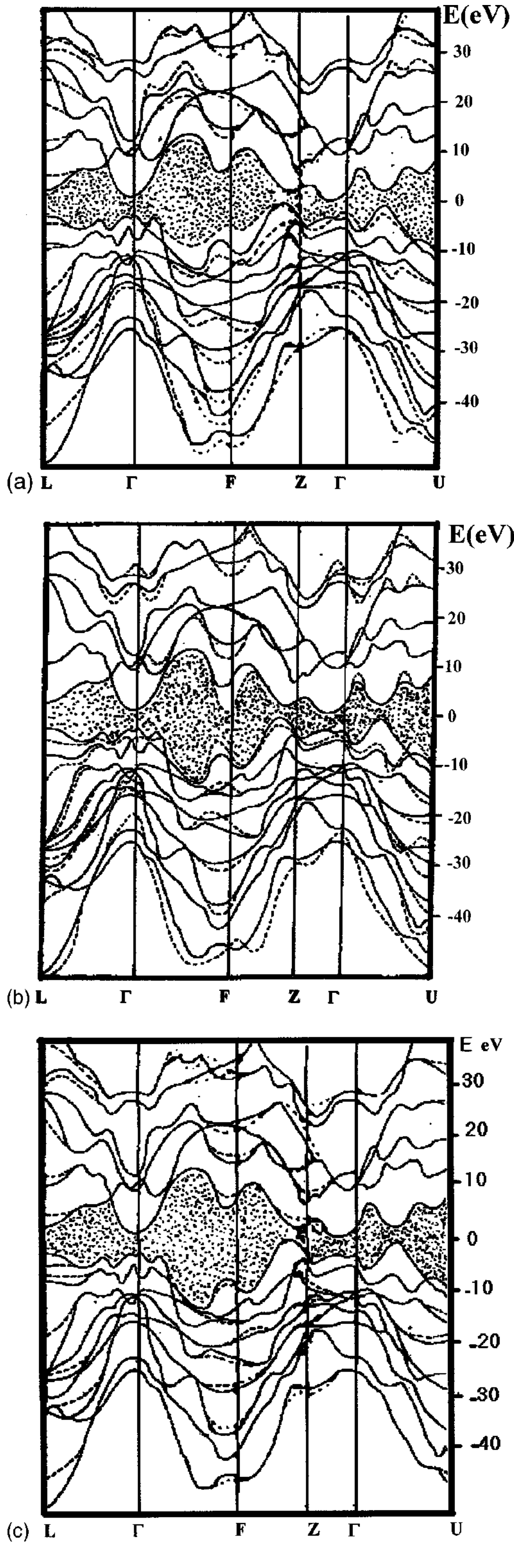

FIG. 4. Band energy structure of the Bi_2Te_3 single crystalline deposited on different substrates: (a) Si⟨111⟩, (b) Si⟨100⟩, and (c) SiO_2.

a proper variational approach with respect to the Perdew-Alder screening parameter.[22] We inserted additional free-carrier charge density in accordance with parameters presented in Table I. The latter leads to a change of the corresponding energy terms and, to a lesser extent, their dispersions.

We have revealed that the pseudopotential (PP) calculated total energy is very sensitive to the energy cutoff and to the screening parameters. In our opinion, such sensitivity is caused by difficulties in properly describing the modulated structure described in Sec. III.

We have thus modified the norm-conserving PP wave functions by their orthogonalization to the lowest combination of atomic orbital (LCAO) wave function. Unfortunately, the different sizes of the basis sets for localized and delocalized wave functions complicate the performance of the self-consistent procedure. The LCAO wave functions were expressed using the Bloch theorem in the case of a real-space representation,

$$\chi_{k,n}(\mathbf{r})=N^{-1/2}\sum_{r}\ \exp(i\mathbf{k}\tau_n)|1,\mathbf{r}-\tau_n\rangle, \tag{3}$$

where $|1\rangle$ is the orbital of the 1-orbital angular momentum symmetry (i.e., s, p, d, f, etc.) and τ_n is the position vector of the nth atom. This technique was described more precisely in the Refs. 23 and 24.

Such a scheme for the orthogonalization allows us to restrict the Hamiltonian diagonalization to a matrix size of 1246. A main iteration criterion to ensure an eigenstate stabilization consists of a coincidence of two neighboring energy eigenvalues within a range of 0.016 eV.

A fitted nonlocal pseudopotential of the one-electron Hamiltonian was expressed as a superposition of the atomiclike $PPV_\alpha(r)$, and was approximated by the expression

$$V_\alpha(r)=(-Z_v e/r)\sum_{i=1}^{n'}\ [c_i\exp(-\alpha_i r^2)+A_i r^2\exp(-\beta_i r^2)], \tag{4}$$

where the fitting coefficients c_i, α_i, A_i, and β_i were calculated on the grounds of a nonlinear interpolation scheme. The set of 8–12 Gaussians was used to provide a good fit of the radial functions in our calculations. All the Hamiltonian matrix elements were decomposed into a series of three-center integrals containing two Gaussians centered at the local atomic positions A and B of the interacting atoms and the atomic potential around the point C. The concrete expressions for the following matrix elements are given in Refs. 23 and 24.

A special point method of Chadhi and Cohen was applied for a calculation of the electronic charge-density distribution. The latter is used to construct a charge-density functional for electrons. The diagonalization procedure was performed at 32 special points of the Brillouin zone (BZ).

A direct iteration process achieved the needed self-consistency. An acceleration of the iteration convergence was obtained by mixing the $(m-1)$th iteration with 68% of the output ρ before their substitution into the next equation. The initial screened potential was constructed using the Thomas-Fermi approximation, that allows one to avoid possible error during the initial electron-density calculation. A criterion of the self-consistency in the charge-density formalism requires that

$$|\rho_{\mathrm{out},m}-\rho_{\mathrm{in},m}|<\varepsilon \tag{5}$$

TABLE II. Structural parameters of the Bi_2Te_3 films deposited on the Si or SiO_2 substrates obtained from the x-ray data and from the molecular-dynamics geometry optimization.

Material	X-ray data, a (Å)	X-ray data, c (Å)	Modulation period along the surface (nm)	Relative modulation amplitude (shift of the atom from the local positions) in the percent
$Bi_2Te_3Si(100)$	4.365	30.238	8.8	0.96
Bi_2Te_3-SiO_2	4.431	30.384	12.3	0.76
Bi_2Te_3-Si(111)	4.364	30.236	8.6	0.93
Si⟨100⟩ deposited on Bi_2Te_3	4.379	30.452	0	0
SiO_2 deposited on Bi_2Te_3	4.401	30.448	0	0

after the mth iteration step. We assume an accuracy of less than $\varepsilon = 0.036\%$ between the input and output iterations as a main criterion for self-consistency (full convergence). The energy eigenvalues were stable within a range of 0.021 eV. The procedure of Hermitic diagonalization was performed using the Querry-limited Jacobi method.

The Hamiltonian was diagonalized at 168 equally spaced points in the $\frac{1}{32}$th part of the BZ to enhance the description precision of the electronic density of states. The numerical evaluations were performed using a tetrahedral method.

The equilibrium dynamic atom positions were obtained from the condition of a minimum of the total-energy electron-density-functional $\rho(r)$. The band-energy calculations were carried out self-consistently after the separation of electron and vibrational degrees of freedom, because in the case of low-energy gaps the influence of electron-phonon interactions is especially high.

The electron-phonon interaction potential was calculated using a nonlinear approximation (similarly to that in Ref. 25). As a consequence we modified all the calculations by an effective renormalization of the electron densities by appropriate electron-phonon states. The role of these *types of interactions* is caused by the low-energy gap of the considered films, and is a consequence of the high thermoactivation occupation.
From these equations we have obtained the modified electron-phonon wave function for a calculation of the band-energy-structure parameters, and have calculated the effective Fermi energy (due both to the electron and phonon subsystems).

B. Results of calculations

The calculated band-energy structures of the Bi_2Te_3 films coated on the different substrates are presented in Fig. 4. In this figure one can see essential band-energy anisotropy between directions perpendicular and parallel to the third-order optical axis ($\Gamma - Z$). Due to the existence of the aforementioned modulated structure originating from interfaces for all the substrates, one can see deviations from the energies in the pure crystallites (in Fig. 4, the main pronounced deviations are denoted by dotted lines). These deviations are varied within 0.1 and 8 eV. Most disturbed are the crystalline films coated on the Si⟨111⟩ substrates [see Fig. 4(a)]. Similar (but slightly weaker disturbances are observed for the Si⟨100⟩ substrates [Fig. 4(b)]. In the case of silica substrates the corresponding changes seem to be essentially smaller [Fig. 4(c)]. This can be explained by the variation of the film structures coating the silicon substrates, presented in Table II. For all three substrates the main changes are predominantly observed in directions along the layers (particularly, $\Gamma - F - U$). This may be a result of differences of the chemical bonds originating from cationic-anionic bonds (covalent-ionic), and the van der Waals interlayer interactions between the anions (the tellur ions).[26] This results in the appearance of highly anisotropic effective masses for the two main crystalline directions.

For all considered cases it is necessary to add that the behavior of the energy bands in the vicinity of the BZ center (point Γ) is practically undisturbed. This confirms the local origin of the observed disturbances, because the center of the

TABLE III. Calculated parameters of the energy gaps, Fermi energy, and averaged band-energy dispersion deviation for the films deposited on different substrates. For comparison (in brackets) we present the same data for Bi_2Te_3 crystals doped with an appropriate number of carriers.

Type of materials	Energy gap (eV)	Fermi energy (eV)	Averaged maximal deviation from pure crystals (eV)
Bi_2Te_3-SiO_2	0.124	−0.081	1.32
	(0.121)	(−0.072)	
Bi_2Te_3-Si(111)	0.123	−0.1184	2.11
	(0.120)	(−0.081)	
Bi_2Te_2-Si(100)	0.123	−0.1211	2.14
	(0.120)	(−0.082)	
Bi_2Te_3 (cryst)	0.119		

TABLE IV. Comparison of the experimentally and theoretically calculated thermopower coefficients and the electro-optics coefficient r_{222}. In the brackets we show results for bulklike Bi_2Te_3 single crystals with the appropriate carrier concentration.

Materials	Theoretical thermoelectric coefficient $\mu_V/T(\mu V/K)$	Experimental thermoelectric $\mu_V/T(\mu V/K)$	EOE tensor (measure) (pm/V)
p-Bi_2Te_3/SiO_2	204 (196)	218	0.75
p-Bi_2Te_3/Si(111)	141 (121)	150	1.12
p-Bi_2Te_3/Si(100)	138 (128)	147	1.14

BZ is connected to the long-range ordering. Moreover, the direction $\Gamma - F$, that is responsible for the Bi-Te chemical bonds, shows a critical dependence on structural modulation even for different Si crystalline cuts. The latter confirms our previous prediction that all substrates first influence the Bi-Te bonds, and are practically insensitive to the interlayer modulation. Generally the features of the band-energy structure (for pure Bi_2Te_3) calculated by us are similar to that calculated in Ref. 9. The main discrepancies appear in a number of valleys in the conduction bands. These can be caused by specific features of the pseudopotential plane waves that are very sensitive to long-range disturbances of the antibonding states comparing with the linear-muffin-tin-orbital basis set. The silicon (silica) substrates disturb not only the higher valence bonding states, originating from the $6p$ Bi$-5p$ Te states, but also the essentially deeper $6s$ Bi-$5p$ Te highly localized corelike bands. This can be explained by the relatively high space delocalization of the mentioned bands.

In Table III we present the main parameters of the band-energy structure obtained by our method for the different substrates. All the data are presented for the carrier concentrations presented in Table I and for p-type doping. For comparison we have made calculations for bulk crystals with appropriate carrier concentrations.

One can see a good agreement of the calculated energy gaps with experimentally measured gaps obtained from the IR absorption and photoconductivity (about 0.152 eV). The SiO_2 substrates shift the Fermi energy to an essentially smaller level compared with the two different crystallographic cuts of the Si crystallites. This is in accordance with the results obtained for deviations of the band energy subbands compared with the bulk crystals. One can see that calculations performed for bulk Bi_2Te_3 crystals doped by an appropriate number of carriers give results that are closer to those for to the bulklike structure than for films. This indicates the central role of the interface band energy gradients in the observed phenomena.

Figure 4(b) clearly shows an essential difference in dispersions of the subbands in Bi_2Te_3 films grown on Si and SiO_2 substrates compared with pure bulk crystals. Moreover one can see that similar deviations (see the brackets in Table III) are observed for a bulk structure doped by an appropriate number of carriers. It is necessary to underline that in the case of the Bi_2Te_3 crystals covered by silicon and silica crystalline films, the changes in the band-energy dispersion are less then 0.2 eV and, as a consequence, do not have so substantial an influence on the behaviors of the composites.

The upper valence band is formed predominantly by $5p$ Te states essentially admixed with highly localized $6s$ Bi states. Such an unusual situation reflects the specific charge transfer (or interlevel hybridization) between the bonding $5p$ Te$-6s$ Bi states effectively interacting with the corresponding electron-phonon subsystem. A strong electrostatic field leads to a shift of the Fermi level. Below, the bonding $5p$ Te$-6s$ Bi is situated delocalized with a high dispersion in $\mathbf{k}$ space. An extremely high dispersion is observed in the Γ-F-U direction.

One of the more sensitive methods to study interface charge transfer in the electron-phonon state is the measurement of the linear electro-optic (Pockels) coefficient described by third-rank polar tensors. This method is very effective for detecting the low portion of the noncentrosymmetry in macrosymmetrical bulk solids. In our case the films are centrosymmetric, and Si substrates are also centrosymmetric. Therefore, for these substrates we can detect changes in the electrostatic potential with a precision up to 0.001 pm (Ref. 27) (for comparison, the reliable best structural analysis gives a possibility of detection of relative electrostatic changes not higher than 0.02 pm).

In Table IV we present calculated data for the electro-optic coefficients r_{222}, and appropriate thermoelectric power coefficients for the different materials. Comparison of the data for experimentally obtained and theoretically calculated electro-optic coefficients r_{222} are presented. Simultaneously we performed calculations of thermoelectric coefficients coming from the parabolic band-energy topology:[28]

$$TE = -(0.6666)\pi^2 k_B^2 T/(2eE_F). \tag{6}$$

The calculated data for the thermoelectric power as well the corresponding experimental data together with the EOE coefficients are presented in Table IV. From Table IV one can clearly see that the experimental data are at least 7–10 % greater as compared with the EOE coefficients. This can be caused both by experimental error as well by neglecting the mesoscopic substructure in our model. More interesting is the correlation with measured EOE coefficients. This fact indicates the central role of the interface carrier charge transfer in the observed thermoelectric properties. From Table IV one can also see the substantial influence of the carrier concentration on the thermoelectric power effects. However, the obtained results indicate that the role of the crystalline interfaces prevails compared with the bulklike contribution.

V. CONCLUSIONS

Using a molecular-dynamics interface structural optimization as well a modified norm-conserving pseudopotential method, the thermoelectric power behavior of Bi_2Te_3 crystalline films grown on Si and SiO_2 substrates was modeled. We have revealed that films with a thickness of 1 μm possess a modulated structure along the layers (perpendicular to optical axis). The period of the modulation is varied within 8 and 12 nm, and is higher for films deposited on Si substrates.

We have shown that the main contribution in the observed effects belongs to states of Bi_2Te_3 single crystalline deposited near the surface on Si crystalline surfaces. If Bi_2Te_3 crystals are used as a substrate, an analogous effect (structural modulation) is observed. This reflects a specific case of modulation of Bi_2Te_3 crystalline films by silicon substrates connected with the difference in the minima of the total energy for these two cases.

The observed modulation may be the main reason for the appearance of crystallitelike islands. We demonstrate a strong dependence between the observed deviations (due to the existence of an interface range) of the energy dispersions and Fermi energy levels and the appropriate thermoelectric power coefficients. The essential role of the electron-phonon subsystem is proved both theoretically (using calculations of the Fermi energy level) as well experimentally by the appearance of electro-optic tensor coefficients r_{222} in the IR spectral range. The proposed approach is essentially powerful when compared with empirical simulations of the ion diffusions and adhesions, because the agreement with experimental data is better.

ACKNOWLEDGMENTS

The authors are grateful to Dr. Ksan Kim (Teoschun University, South Korea) for the possibility of measuring the Bi_2Te_3 crystals covered by different substrates.

[1] I. J. Osugi, T. Kojima, M. Sakata, M. Yamanashi, and I. A. Nishida, J. Appl. Phys. **76**, 2235 (1994).
[2] K. Watanabe, N. Sato, and S. Miyaka, J. Appl. Phys. **54**, 1256 (1983).
[3] S. Murata, H. Nakada, T. Abe, H. Tanaka, and A. Watabe, Jpn. J. Appl. Phys. **32**, 5284 (1993).
[4] L. D. Hicks and M. S. Dresselhaus, Phys. Rev. B **47**, 12 727 (1993).
[5] D. J. Singh and W. E. Pickett, Phys. Rev. B **50**, 11 235 (1994).
[6] B. C. Sales, D. Mandrus, and R. K. Williams, Science **272**, 1325 (1996).
[7] E. V. Oleshko and V. N. Korolyshin, Fiz. Tverd. Tela (Leningrad) **27**, 2856 (1985) [Sov. Phys. Solid State **27**, 1723 (1985)].
[8] G. A. Thomas, D. H. Rapkine, R. B. van Dover, L. F. Mattheiss, W. A. Sundere, W. A. Schneemeyer, and J. V. Waszczak, Phys. Rev. B **46**, 1553 (1992).
[9] S. K. Mishra, S. Satpathy, and O. Jepsen, J. Phys.: Condens. Matter **9**, 461 (1997).
[10] M. Ferhat, B. Liautard, G. Brun, J. C. Tedenac, M. Nouaoura, and L. Lassabatere, J. Cryst. Growth **167**, 122 (1996).
[11] E. H. Kaddouri, T. Maurice, X. Gratens, S. Charar, S. Benet, A. Mefleh, J. C. Tedenac, and B. Liautard, Phys. Status Solidi (1999).
[12] Y. A. Boikov, O. S. Gribanowa, V. A. Danilov, and A. Kutasov, Fiz. Tverd. Tela (Leningrad) **33**, 3414 (1991) [Sov. Phys. Solid State **33**, 1926 (1991)].
[13] I. V. Kityk, Phys. Crystallogr. (USA) **35**, 458 (1990).
[14] C. G. Broyden, J. Inst. Math. Appl. **6**, 222 (1970).
[15] R. Fletcher, Comput. J. (Switzerland) **13**, 317 (1970); D. Goldfarb, Math. Comput. **24**, (1970).
[16] D. F. Shanoo, Math. Comput. **24**, 647 (1970).
[17] A. D. Becke, J. Chem. Phys. **98**, 1372 (1994); **98**, 5648 (1994).
[18] G. E. Franklin, S. Tang, J. C. Woicik, M. J. Bedzyk, A. J. Freeman, and J. A. Golovchenko, Phys. Rev. B **52**, R5515 (1995).
[19] R. W. G. Wyckoff, *Crystal Structures* (Krieger, Malabar, FL, 1986), Vol. 2.
[20] G. Bachelet, D. R. Hamann, and M. Schluter, Phys. Rev. B **26**, 4199 (1982).
[21] A. S. Krochuk, I. V. Kityk, and M. I. Kolinko, J. Phys. Chem. Solids **53**, 1315 (1992).
[22] J. Perdew and A. Zunger, Phys. Rev. B **23**, 5048 (1981).
[23] I. V. Kityk, J. Kasperczyk, and B. V. Andrievskii, Phys. Lett. **216A**, 161 (1996).
[24] M. Malachowski, I. R. Kityk, and B. Sahraoui, Phys. Status Solidi B **207**, 405 (1998).
[25] I. V. Kityk and B. Sahraoui, Phys. Rev. B **60**, 942 (1999).
[26] P. Pecheur and G. Toussaint, Phys. Lett. **135A**, 223 (1989).
[27] I. V. Kityk, Solid State Phys. **33**, 1026 (1991).
[28] D. K. C. MacDonald, *Thermoelectricity* (Wiley, New York, 1962), p. 25.